

Synthesis of Li^+ adsorbent (H_2TiO_3) and its adsorption properties

Xi-chang SHI, Zhi-bing ZHANG, Ding-fang ZHOU, Li-fen ZHANG, Bai-zhen CHEN, Liang-liang YU

School of Metallurgical Science and Engineering, Central South University, Changsha 410083, China

Received 31 December 2011; accepted 4 May 2012

Abstract: H_2TiO_3 was obtained from the acid-modified adsorbent precursor Li_2TiO_3 , which was synthesized by a solid-phase reaction between TiO_2 and Li_2CO_3 . The extraction ratio of Li^+ from Li_2TiO_3 was 98.86%, almost with no Ti^{4+} extracted. The effects of lithium titanium ratio, calcining temperature and time were investigated on the synthesis of Li_2TiO_3 . Li_2TiO_3 , H_2TiO_3 and the adsorbed Li^+ adsorbent were characterized by XRD and SEM. The lithium adsorption properties were investigated by the adsorption kinetics and adsorption isotherm. The results indicate that H_2TiO_3 has an excellent adsorptive capacity for Li^+ . Two simplified kinetic models including the pseudo-first-order and pseudo-second-order equations were selected to follow the adsorption processes. The rate constants of adsorption for these kinetic models were calculated. The results show that the adsorption process can be described by the pseudo-second-order equation, and the process is proved to be a chemical adsorption. The adsorption process that H_2TiO_3 adsorbs Li^+ in LiCl solution well fits the Langmuir equation with monolayer adsorption.

Key words: Li^+ adsorbent; Li_2TiO_3 ; adsorption property; kinetic models; monolayer adsorption; TiO_2 ; Li_2CO_3

1 Introduction

Traditional precipitation, solvent extraction and salting method [1,2] are not suitable for a small amounts of Li-containing sea water and salt lake brine on lithium extraction. A new separating technique [3,4] of alkali and alkaline metals with similar nature benefits from the inorganic separation material with ion function memory. At present, the study of lithium ionic sieve is mainly focused on manganese lithium ionic sieve [5–7], which exists in the disfigurement of few cyclic number and big dissolved loss etc. Titanium lithium ionic sieve has some remarkable advantages, such as less dissolved loss and stable structure. $\text{Li}_4\text{Ti}_5\text{O}_{12}$ was synthesized by the sol–gel method [8,9] and the lithium ionic sieve was obtained after acid treatment. The pull-out rate of lithium reached 81.5%, while that of titanium ion was below 4.2%. The adsorptive capacity for lithium ion reached 42.30 mg/g. Li_2TiO_3 was obtained via the solid phase synthesis method [10–12] with mixed crystal titanium dioxide (anatase content was 83.1%) as raw material and lithium ionic sieve was acquired after pickling. Its saturated adsorptive capacity came up to 28.76 mg/g. Li_2TiO_3 had a special separation effect on lithium in the

brine gas field with high calcium and magnesium but low lithium. It can be seen that the form of titanium dioxide used has a great influence on the adsorption performance of Li_2TiO_3 , which was used as the lithium adsorbent precursor.

In this work, Li_2TiO_3 was synthesized by a solid-phase method with mixed crystal titanium dioxide. Then lithium adsorbent (H_2TiO_3) was obtained by pickling with hydrochloric acid. The structure characteristics and ion-exchange properties were studied by XRD, SEM, Li^+ adsorption isotherm, kinetics and adsorption measurement, respectively.

2 Experimental

The experimental technology process is shown in Fig. 1. The lithium adsorbent precursor was synthesized by a solid-phase reaction between TiO_2 and Li_2CO_3 . Prior to calcination, the mixture of TiO_2 and Li_2CO_3 was milled and blent with anhydrous alcohol as dispersant. Then it was dried at 100 °C for 2 h. Finally, the dried mixture was calcined at 850 °C for 24 h and pickled with hydrochloric acid. The adsorbent was used to adsorb lithium ion in solution, then it was regenerated with hydrochloric acid.

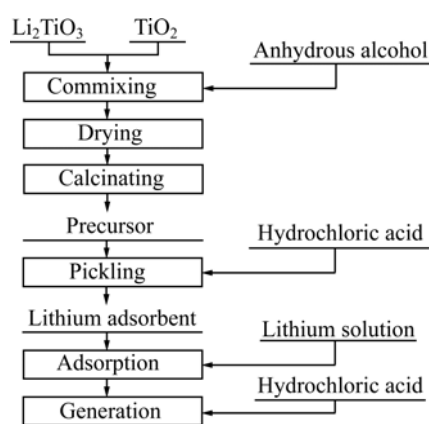


Fig. 1 Flow chart of experimental process

3 Results and discussion

3.1 Synthesis of lithium adsorbent precursor (Li_2TiO_3)

The XRD patterns of Li_2TiO_3 synthesized under different lithium titanium ratios ($R=2.00, 2.04, 2.10, 2.16$) with Li_2CO_3 and TiO_2 are shown in Fig. 2. The results indicate the pure phase of Li_2TiO_3 can be obtained under all ratios. The intensities of diffraction peaks increase with increasing the lithium titanium ratio, which indicates that the crystal shape is more complete under a higher lithium to titanium ratio.

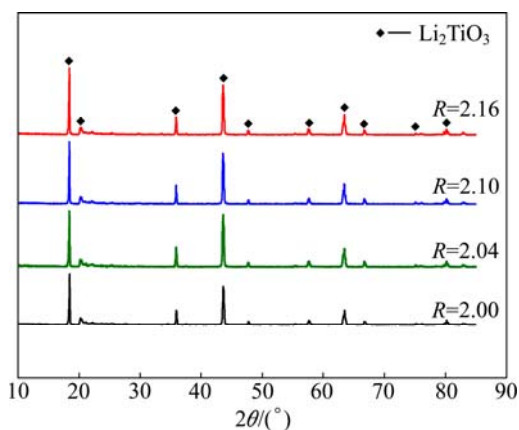


Fig. 2 XRD patterns of Li_2TiO_3 synthesized with different titanium to lithium ratios

3.1.1 Lithium to titanium ratio

The effect of lithium to titanium ratio ($R=n(\text{Li})/n(\text{Ti}), 2.00, 2.04, 2.08, 2.10, 2.14, 2.16$) on lithium extraction and titanium dissolved loss rate is shown in Fig. 3. Under the same pickling conditions (0.25 mol/L HCl, 60 °C), lithium drawn out reduces with the increasing of R . The extraction rate of lithium is 85.62% when R is 2, but it is reduced to 77.87% at $R=2.16$. In contrast, the dissolved loss rate of titanium increases slowly with the increasing of R , which is 0.17% when R is 2 and it is increased to 0.34% at $R=2.16$. Figure 4 shows the effect of R on the adsorptive capacity. As can

be seen from Fig. 4 the adsorptive capacity decreases with an increase of R under the same pickling and adsorption conditions. The adsorptive capacity is 25 mg/g when R is 2 and decreases to 11.8 mg/g when R increases to 2.16. This indicates that the crystal structure of Li_2TiO_3 becomes more complete and stable with the increase of R , which is consistent with that in Fig. 2. According to lithium extraction, titanium dissolution loss rate and adsorptive capacity, the optimum chemical ratio is chosen as 2.

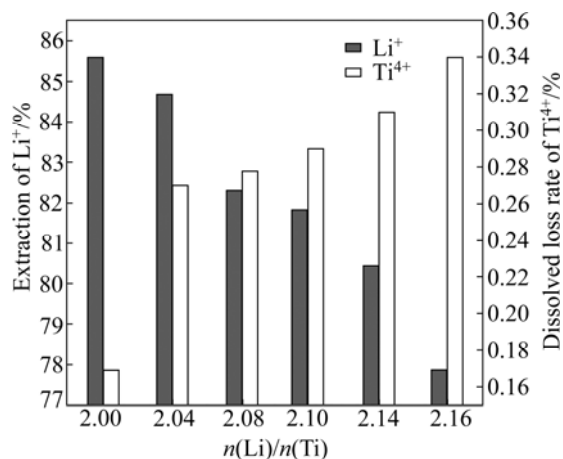


Fig. 3 Effects of lithium to titanium mole ratio on lithium extraction and titanium dissolved loss rate

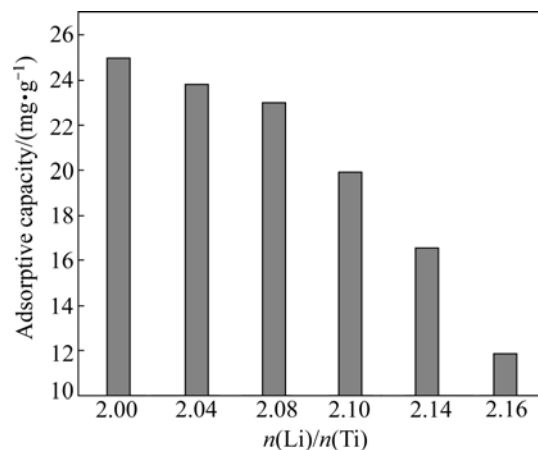


Fig. 4 Effect of lithium to titanium mole ratio on adsorptive capacity

3.1.2 Synthesis temperature

Figure 5 shows the effects of temperature on the XRD patterns of lithium adsorbent precursor obtained under the conditions of lithium to titanium ratio of 2 and calcining time of 24 h. The pure phase of Li_2TiO_3 can be synthesized from 550 °C to 1050 °C. All diffraction peak intensities increases with the synthesis temperature increased from 550 °C to 850 °C, which illustrates that the crystal structure of Li_2TiO_3 becomes more complete with increasing the temperature. The results show that all the diffraction peak intensities become weak gradually

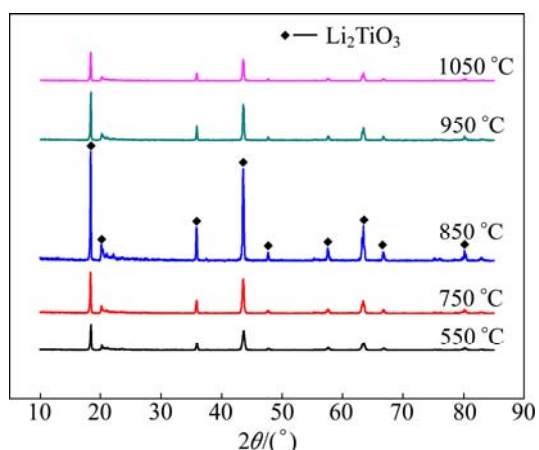


Fig. 5 XRD patterns of Li_2TiO_3 synthesized at different temperatures

when the temperature is higher than 850 °C. According to Refs. [13–15], the single inclined crystal of Li_2TiO_3 is converted into the cubic crystal when the temperature is higher than 1150 °C. It can be concluded that the structural change stage happened when the temperature is higher than 850 °C, which leads to a weaker diffraction peak intensity.

Figure 6 shows the effect of synthesis temperature on lithium extraction and titanium dissolved loss rate. Lithium extraction rate decreases with the increase of synthesis temperature under the same pickling conditions (0.25 mol/L HCl, 60 °C). The rates of lithium elicited are 88.31%, 85.62% and 56.21% at synthesis temperatures of 550, 850 and 1050 °C, respectively. The titanium dissolved loss rate increases with the increase of synthesis temperature. The titanium dissolved loss rates are 0.15%, 0.17% and 1.16% at synthesis temperatures of 550, 850 and 1050 °C, respectively.

The lithium adsorbent adsorptive capacity shows little dependence on temperature in the range of 550–850 °C, as shown in Fig. 7. The adsorptive capacities are

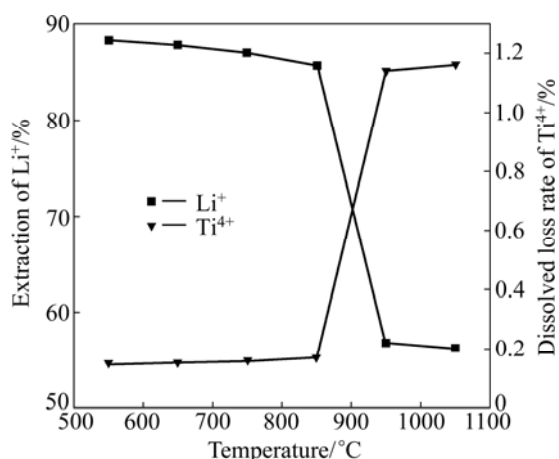


Fig. 6 Effects of synthesis temperature on lithium extraction and titanium dissolved loss rate

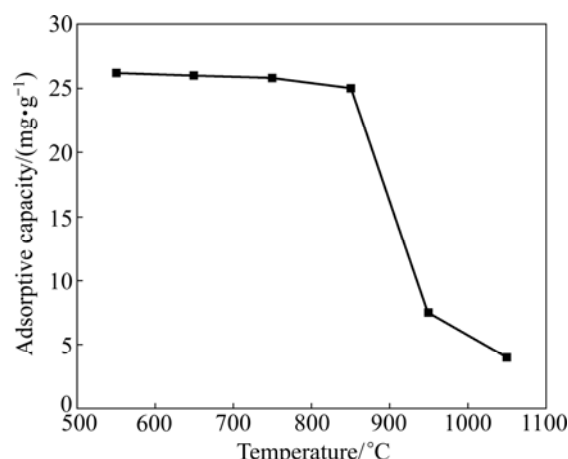


Fig. 7 Effect of synthesis temperature on lithium adsorptive capacity

26.2 and 25 mg/g at 550 °C and 850 °, respectively. When the temperature is 1050 °C, the adsorption capacity decreases sharply to 4 mg/g. It can be concluded that the suitable synthesis temperature is between 550 °C and 850 °C by considering the lithium extraction rate, titanium dissolved loss rate and lithium adsorptive capacity comprehensively.

3.2 Preparation and characterization of lithium adsorbent (H_2TiO_3)

Lithium adsorbent (H_2TiO_3) was obtained when the lithium adsorbent precursor was treated with hydrochloric acid. Figure 8 shows the relationship between the lithium extraction and the extracting time. As can be seen from Fig. 8, the rate of lithium extracted reached 83.64% when Li_2TiO_3 was treated by pickling for 24 h. Then it increased slowly with the extension of time, so it reached 98.86% after 96 h. While the content of the titanium ion in solution was almost zero through spectrophotometry method, which suggests that titanium is almost insoluble loss in the pickling process.

Figure 9 shows XRD patterns of Li_2TiO_3 , H_2TiO_3 before and after adsorbing Li^+ . Figure 9(a) shows XRD

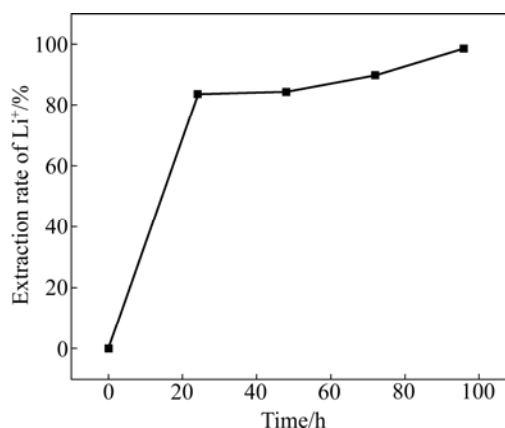


Fig. 8 Variation of Li^+ extraction rate with reaction time

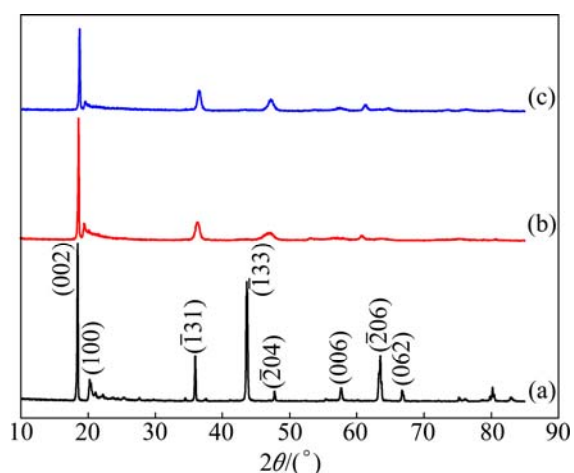


Fig. 9 XRD patterns of Li_2TiO_3 (a), H_2TiO_3 before (b) and after (c) adsorbing Li^+

patterns of pure monoclinic crystal of Li_2TiO_3 (the lattice constant: $a=0.5069$ nm, $b=0.8799$ nm, $c=0.9759$ nm, JCPDS 33—831). The pattern in Fig. 9(b) shows that the diffraction peak shifts to right and the strength weakens significantly compared with the pattern in Fig. 9(a). The diffraction peaks of pattern become wide. All of the changes indicate that hydrogen ions (radius is about 0.0012 nm) exchange with lithium atoms (radius is about 0.076 nm) when Li_2TiO_3 is treated with acid. The crystal interplanar spacing becomes narrow and the grains become small after treatment. It can be seen that the XRD pattern in Fig. 9(c) is alike with that in Fig. 9(b), which suggests that the structure does not change much after absorption.

Figure 10 shows the SEM images of Li_2TiO_3 , H_2TiO_3 before and after adsorbing Li^+ . It can be seen from Fig. 10, Li_2TiO_3 obtained by solid-phase synthesis method is comparatively uniform, with the particle size of 1–2 μm . Figures 10(b) and (c) show the particles with some irregular crackles.

3.3 Adsorptive properties

3.3.1 Saturated adsorptive capacity

Figure 11 shows the adsorptive capacity of lithium adsorbent (H_2TiO_3) in LiOH solution of 694.1 mg/L Li^+ , LiCl solution of 282.5 mg/L Li^+ and 87.5 mg/L Li^+ . The results show that the adsorptive capacity increases with the increase of time in LiOH or LiCl solution. The adsorptive capacity increases quickly in the first 24 h and then increases slowly with prolonging time. Finally, it reaches a plateau after 192 h. The adsorptive capacities are 39.8, 30.9 and 28.63 mg/g in deferent solutions described above, respectively. The results indicate that the absorbent has strong adsorption ability to lithium in the alkaline solution. The adsorption reaction is as follows: $\text{H}_2\text{TiO}_3 + \text{Li}^+ \rightarrow \text{Li}_2\text{TiO}_3 + \text{H}^+$. H^+ was released and

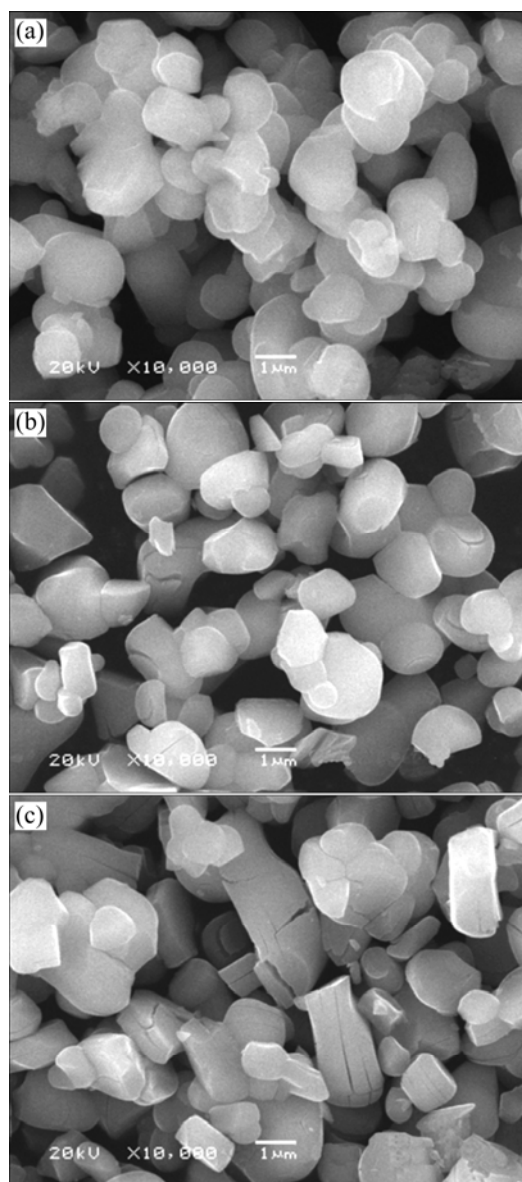


Fig. 10 SEM images of Li_2TiO_3 (a), H_2TiO_3 before (b) and after (c) adsorbing Li^+

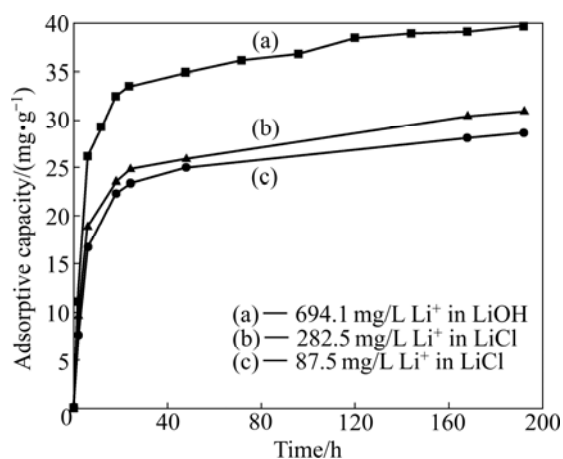


Fig. 11 Variation of adsorptive capacity with time

OH⁻ was consumed constantly when lithium ion in the solution was adsorbed constantly. The adsorptive capacity increased slowly until the adsorption balance reached with the extension of time. Thus the adsorptive capacity in LiOH solution was more than that in LiCl solution, which was also concluded by AYDIN et al [16] and MARTIN et al [17].

3.3.2 Adsorption dynamics

The lithium generally exists in the form of LiCl in saline brine, so the adsorption dynamics that the adsorbent adsorbed in LiCl solution with different concentrations was investigated. There were many reports about the adsorption dynamics research of adsorbent for metal ions. At present, the pseudo-first-order (equation 1) and pseudo-second-order (equation 2) kinetic models are widely used to study the adsorption mechanism and determine the rate constant of adsorption process [18–20]:

$$\lg(q_e - q_t) = \lg q_e - \frac{k_{ad}}{2.303} \times t \tag{1}$$

$$\frac{t}{q_t} = \frac{1}{kq_e^2} + \frac{1}{q_e} \times t \tag{2}$$

where q_e and q_t are the adsorbent adsorptive capacities to Li⁺ at adsorption equilibrium and any time t , respectively; k_{ad} and k are the rate constants of the pseudo-first-order and pseudo-second-order kinetic models, respectively.

The curves b and c in Fig. 11 are made a linear fitting with the pseudo-first-order and pseudo-second-order dynamic equations, and the results are shown in Fig. 12 and Table 1. As shown in Fig. 12 and Table 1, the

linear correlation coefficient of the pseudo-second-order dynamic equation is 0.999, which is greater than that of the pseudo-first-order dynamic equation. Thus it can be concluded that the adsorption dynamics in LiCl solution is conformed to the pseudo-second-order kinetic model. Some important kinetic parameters can be calculated by the pseudo-second-order dynamic equation. For example, the rate constants at the two concentrations are 0.00574 and 0.0051 g/(mg·h), respectively. The equilibrium adsorptive capacities are 29.32 and 31.63 mg/g. The adsorptive capacities are fairly near 28.63, 30.9 mg/g according to Fig. 11, respectively. This further confirms the conclusion that the adsorption in LiCl solution conforms to the pseudo-second-order dynamic equation and the adsorption process is mainly a chemical adsorption [21].

3.3.3 Adsorption isotherm

The experimental data were analyzed by the Langmuir and Freundlich models [22], the equations of which can be expressed as

$$\frac{\rho_e}{q_e} = \frac{1}{q_m} \rho_e + \frac{1}{K_L q_m} \tag{3}$$

$$\lg q_e = \frac{1}{n} \lg \rho_e + \lg K_F \tag{4}$$

where ρ_e is the equilibrium concentration of Li⁺ solution; q_e is the equilibrium adsorptive capacity of Li⁺; q_m is the theoretical maximum adsorptive capacity of Li⁺; K_L is the Langmuir empirical constant; n and K_F are the Freundlich constants indicating relative adsorptive capacity and adsorption rate, respectively.

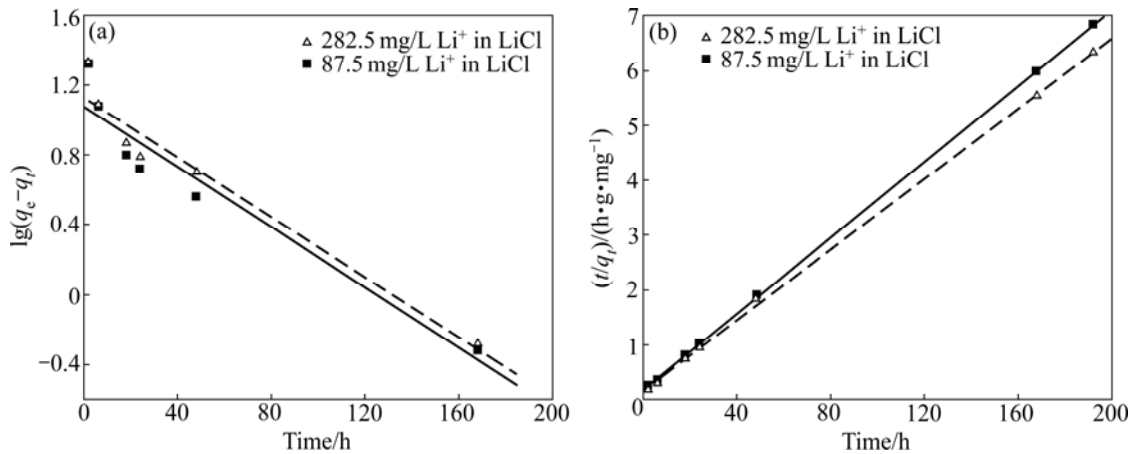


Fig. 12 Pseudo-first-order (a) and pseudo-second-order (b) kinetic plots for Li⁺ adsorption at different Li⁺ concentrations

Table 1 Kinetic parameters for Li⁺ adsorption at different concentrations

$\rho_{Li^+}/(mg \cdot L^{-1})$	$q_e(\text{exp.})/(mg \cdot g^{-1})$	Pseudo-first-order			Pseudo-second-order		
		k_{ad}/h^{-1}	$q_e(\text{theor.})/(mg \cdot g^{-1})$	R^2	$k/(g \cdot mg^{-1} \cdot h^{-1})$	$q_e(\text{theor.})/(mg \cdot g^{-1})$	R^2
87.5	28.63	0.01988	11.89	0.9217	0.00574	29.32	0.9997
282.5	30.90	0.01974	13.35	0.9477	0.0051	31.63	0.9992

The equilibrium concentration of Li^+ and adsorptive capacity of adsorbent in LiCl solution of different concentrations were fitted linearly with Langmuir and Freundlich models. The results are shown in Fig. 13 and Table 2. The linear correlation coefficient of Langmuir model reaches 0.9984, which is much greater than that of Freundlich model. This indicates the adsorption of adsorbent for Li^+ conforms to Langmuir model. It is a monolayer adsorption and the maximum absorption capacity is 37.01 mg/g.

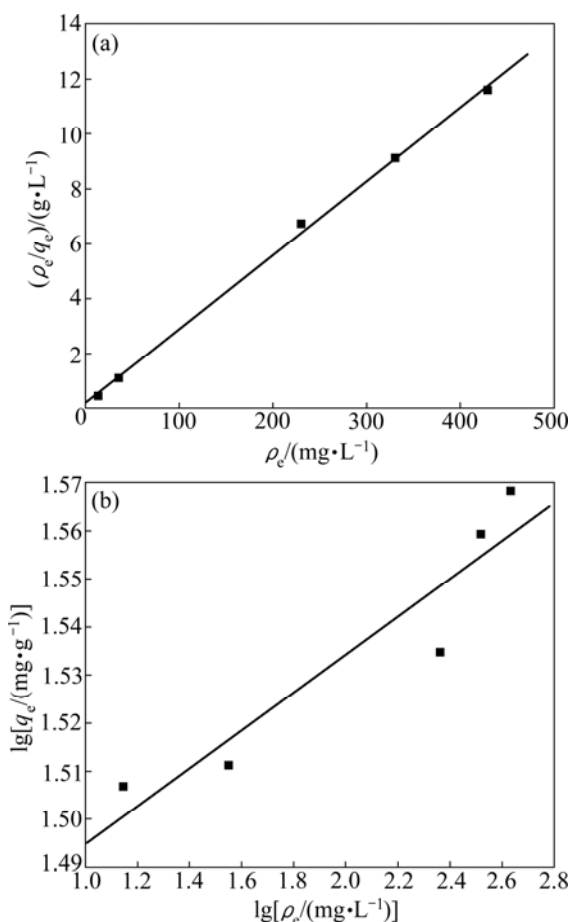


Fig. 13 Langmuir (a) and Freundlich (b) isotherms in LiCl solution of different concentrations

Table 2 Type and parameters of isothermal adsorption of Li^+ -adsorbent

Langmuir			Freundlich		
$q_m/$ ($\text{mg}\cdot\text{g}^{-1}$)	$K_L/$ ($\text{L}\cdot\text{mg}^{-1}$)	R^2	n	$K_F/$ ($\text{L}\cdot\text{g}^{-1}$)	R^2
37.01	0.15333	0.9984	25.3229	28.5351	0.8814

3.3.4 Peculiarity of selective adsorbent to lithium ion

The lithium adsorbent was placed in the salt lake brine to make a cycle experiment and carry a study on the separation properties of adsorbent for the main metal ions in it. Table 3 lists the separation coefficients of lithium ion to several main metal ions in brine. As can be

seen from Table 3, the adsorbent has better separation properties of Li^+ to Na^+ , K^+ and Mg^{2+} , but the separation coefficient is not very large, which is related with the adsorption time and the nature of brine. In the brine, the content of Li^+ is low, while that of Na^+ , K^+ or Mg^{2+} is very high. The separation coefficient becomes more and more with the cycle carrying. This indicates that the increase of cycle times is beneficial to the separation of Li^+ to K^+ , Na^+ and Mg^{2+} in salt lake brine. The separation coefficient of lithium to magnesium reaches 102.40 at the 8th adsorption, which can be a good separation of lithium and magnesium ions in salt lake brine.

Table 3 Separation coefficients of lithium ion to several main metal ions in brine

Designation	Separation coefficient		
	$\alpha_{\text{K}}^{\text{Li}}$	$\alpha_{\text{Na}}^{\text{Li}}$	$\alpha_{\text{Mg}}^{\text{Li}}$
1st adsorption	16.36	15.38	12.87
5th adsorption	29.51	26.97	27.75
8th adsorption	30.98	29.46	102.40

4 Conclusions

1) A single crystal phase of Li_2TiO_3 can be synthesized by solid method using titanium dioxide and lithium carbonate as raw materials. Optimization preparation conditions of metatitanate lithium precursor are: lithium to titanium ratio of 2, synthesis temperature of 850 °C and synthesis time of 24 h.

2) Lithium adsorbent (H_2TiO_3) can be obtained after pickling Li_2TiO_3 with hydrochloric acid. The extraction ratio of Li^+ from Li_2TiO_3 reached 98.86%, and the rate of titanium dissolved loss was only 0.17%.

3) Lithium adsorbent (H_2TiO_3) has an excellent adsorption ability to Li^+ . The equilibrium adsorptive capacity in LiOH solution containing 694.1 mg/L Li^+ reached 39.8 mg/g.

4) The adsorption process that H_2TiO_3 adsorbs Li^+ in LiCl solution conformed to the pseudo-second-order dynamic equation, which shows that the adsorption process is mainly chemical adsorption. What's more, the adsorption process also conformed to Langmuir model, which shows that the adsorption process is monolayer absorption.

5) The separation coefficient of lithium to magnesium reaches 102.4 at the 8th adsorption, which can be a good separation of lithium and magnesium ions in salt lake brine.

References

- [1] VAN G S W, TANG Y, RITTMANN B E. Impact of precipitation on the treatment of real ion-exchange brine using the H_2 -based membrane biofilm reactor [J]. Water Sci Technol, 2011, 63(7):

- 1453–1458.
- [2] HAMZAOUI A H, HAMMI H, MNIF A. Operating conditions for lithium recovery from natural brines [J]. *Russ J Inorg Chem*, 2007, 52(12): 1859–1863.
- [3] YANG S T, KIM J, AHN W S. CO₂ adsorption over ion-exchanged zeolite beta with alkali and alkaline earth metal ions [J]. *Microporous Mesoporous Mat*, 2010, 135(1–3): 90–94.
- [4] BRUZZONITI M C, CARLO R M D, FIORILLI S, ONIDA B, SARZANINI C. Functionalized SBA-15 mesoporous silica in ion chromatography of alkali, alkaline earths, ammonium and transition metal ions [J]. *J Chromatogr A*, 2009, 1216(29): 5540–5547.
- [5] WANG L, MENG C G, MA W. Study on Li⁺ uptake by lithium ion-sieve via the pH technique [J]. *Colloid Surf A*, 2009, 334(1–3): 34–39.
- [6] ZHANG Q H, SUN S Y, LI S P, JIANG H, YU J G. Adsorption of lithium ions on novel nanocrystal MnO₂ [J]. *Chem Eng Sci*, 2007, 62(18–20): 4869–4874.
- [7] WANG L, MA W, LIU R, LI H Y, MENG C G. Correlation between Li⁺ adsorption capacity and the preparation conditions of spinel lithium manganese precursor [J]. *Solid State Ionics*, 2006, 177(17–18): 1421–1428.
- [8] XIANG H F, TIAN B B, LIAN P C, LI Z, WANG H H. Sol-gel synthesis and electrochemical performance of Li₄Ti₅O₁₂/graphene composite anode for lithium-ion batteries [J]. *J Alloy Compd*, 2011, 509(26): 7205–7209.
- [9] WANG D, DING N, SONG X H, CHEN C H. A simple gel route to synthesize nano-Li₄Ti₅O₁₂ as a high-performance anode material for Li-ion batteries [J]. *J Mater Sci*, 2009, 44(1): 198–203.
- [10] SINHA A, NAIR S R AND SINHA P K. Single step synthesis of Li₂TiO₃ powder [J]. *J Nucl Mater*, 2010, 399(2–3): 162–166.
- [11] ZHONG Hui. Property of H₂TiO₃ type ion-exchangers and extraction of lithium from brine of natural gas wells [J]. *Chinese Journal of Applied Chemistry*, 2000, 17(3): 307–309. (in Chinese)
- [12] DEPTULA A, OLCZAK T, LADA W, SARTOWSKA B, CHMIELEWSKI A G, ALVANI C, CARCONI P L, BARTOLOMEO A D, PIERDOMINICI F, CASADIO S. Fabrication of Li₂TiO₃ spherical microparticles from TiCl₄ by a classical, inorganic sol-gel route; Characteristics and tritium release properties [J]. *J Mater Sci*, 2002, 37(12): 2549–2556.
- [13] KATAOKA K, TAKAHASHI Y, KIJIMA N, NAGAI H, AKIMOTO J, IDEMOTO Y, OHSHIMA K. Crystal growth and structure refinement of monoclinic Li₂TiO₃ [J]. *Mater Res Bull*, 2009, 44(1): 168–172.
- [14] KLEYKAMP H. Heat capacity and enthalpy of transformation of Li₂TiO₃ [J]. *J Nucl Mater*, 2001, 295(2–3): 244–248.
- [15] KLEYKAMP H. Phase equilibria in the Li-Ti-O system and physical properties of Li₂TiO₃ [J]. *Fusion Eng Des*, 2002, 61–62: 361–366.
- [16] AYDIN F, YASAR F, AYDIN I, GUZEL F. Determination of lead separated selectively with ion exchange method from solution onto BCW in Sirtak, East Anatolia of Turkey [J]. *Microchem J*, 2011, 98(2): 246–253.
- [17] MARTIN M H, LASIA A. Study of the hydrogen absorption in Pd in alkaline solution [J]. *Electrochim Acta*, 2008, 53(22): 6317–6322.
- [18] ZHOU L M, WANG Y P, LIU Z R, HUANG Q W. Characteristics of equilibrium, kinetics studies for adsorption of Hg(II), Cu(II), and Ni(II) ions by thiourea-modified magnetic chitosan microspheres [J]. *Hazardous Materials*, 2009, 161(2): 995–1002.
- [19] BENHAMMOU A, YAACOUBI A, NIBOU L, TANOUTI B. Adsorption of metal ions onto Moroccan stevensite: Kinetic and isotherm studies [J]. *J Colloid Interface Sci*, 2005, 282(2): 320–326.
- [20] BARKAT M, NIBOU D, CHEGROUCHE S, MELLAH A. Kinetics and thermodynamics studies of chromium (VI) ions adsorption onto activated carbon from aqueous solutions [J]. *Chem Eng Process*, 2009, 48(1): 38–47.
- [21] NAIYA T K, BHATTACHARYA A K, DAS S K. Removal of Cd(II) from aqueous solutions using clarified sludge [J]. *J Colloid Interface Sci*, 2008, 325(1): 48–56.
- [22] WANG L, MENG C G, HAN M, MA W. Lithium uptake in fixed-pH solution by ion sieves [J]. *J Colloid Interface Sci*, 2008, 325: 31–40.

锂离子吸附剂(H₂TiO₃)的合成及吸附性能

石西昌, 张志兵, 周定方, 张丽芬, 陈白珍, 余亮良

中南大学 冶金科学与工程学院, 长沙 410083

摘要: 选取 TiO₂ 为钛源、Li₂CO₃ 为锂源, 采用高温固相法合成锂吸附剂前驱体 Li₂TiO₃, 并探讨锂钛比、焙烧温度、焙烧时间等因素对合成 Li₂TiO₃ 性质的影响。将 Li₂TiO₃ 用一定浓度的盐酸酸洗脱锂后制得偏钛酸型锂吸附剂 H₂TiO₃, 酸洗过程中锂的抽出率达到 98.86%, 而离子筛中的钛溶损却很小。采用 XRD 和 SEM 等分析手段对 TiO₂、Li₂TiO₃ 和 H₂TiO₃ 及其吸附锂后的样品进行表征。最后应用伪一级和伪二级动力学方程对 H₂TiO₃ 的吸附性能进行研究, 并对吸附过程进行拟合从而计算相应的速率常数。结果表明: H₂TiO₃ 对锂离子具有较大的吸附能力, 吸附过程符合伪二级动力学方程, 表明吸附过程主要为化学吸附; 在 LiCl 溶液中的吸附平衡数据符合 Langmuir 等温吸附方程, 表明吸附过程为单层吸附。

关键词: 锂离子吸附剂; Li₂TiO₃; 吸附性能; 动力学模型; 单层吸附; TiO₂; Li₂CO₃

(Edited by Hua YANG)